AN IMPROVED COUNTERBALANCE MECHANISM FOR A 3-DOF MANIPULATOR

Minh Nhut Nguyen, Tri Cong Phung
Ho Chi Minh City University of Technology, VNU-HCM, Vietnam

Received 01/11/2018, Peer reviewed 29/11/2018, Accepted for publication 27/02/2019

ABSTRACT

This paper describes an improved counterbalance mechanism fitting with the common structure of industrial robot arms. We have also developed three degree of freedom (DOF) manipulator, whose structural design resembles industrial robots, aiming to apply Lead-through programming. To verify the mechanism, the robot was designed to carry a load of 3 kg at the end of effector, which is equivalent to a concentrated weight of last three DOFs having type of spherical wrists. As a result, the robot can remain any postures in its workspace even maximum horizontal reach without auxiliary actuators. Furthermore, the robot was handled successfully to be programmed by Lead-through method. In summary, the improvement is practical for general industrial robots.

Keywords: *Lead-through programming; improved counterbalance mechanism; 3-DOF manipulator; industrial robots; common structure.*

1. INTRODUCTION

The Lead-through technique is a common control method of industrial robot programming. This technique is appropriate to small-sized and medium-sized industrial manipulators, helping operators save much time in programming. Robots with the technique are suitable to program continuous motion, and also reduce the time for positioning points in point-to-point motion. The possibility of quick and intuitive programming is achieved by manually moving the end-effector through desired points and recording them.

When designing a robot to use Lead-through programming, a decisive factor to the robot's capacity is the structure of first three DOFs, called position structures, which play an important role in positioning a wrist. There is a variety of configurations, but the most popular one is the anthropomorphic structure due to a large workplace volume in comparison with their encumbrance [5]. In addition, the typical structures of the first three revolute joints of an anthropomorphic are the type of roll-pitch-pitch joints. Basically, pitch joints are influenced significantly by gravity due to links mass. Thus, motors required to drive pitch joints are also more powerful with high torque, which also increase their price, and drivetrain in size.

Researchers have proposed and developed many counterbalance mechanisms to cope with the problem. In some types of industrial robots, motors are mounted at opposite ends of links, where their weights are used as counterweights. However, the disposition as above makes drivetrain complicated. Gravity counterbalancing can be achieved by a zero-length spring. Normal springs in combination with auxiliary mechanisms, such as crank – slider [1], cable – pulley [2], [3] , wire – slider [4] was proposed and developed to compensate gravity torque.

Nevertheless, kinematics models which were utilized in these studies were idealized to verify the feasibility of the proposed methods. Practically, real structures of industrial robots are different from the experimental ones in order to facilitate the

arrangement of the fourth motor, engendering a change in kinematics model. In the paper, we take into account our robot's kinematics model to improve the gravity counterbalance mechanism to achieve a self-balanced robot.

In the rest of the paper, the content is organized as follows. Section 2 discusses the problem of a counterbalance mechanism, and the limitation when being applied to a real manipulator structure. In section 3, we improve the mechanism to solve the problem. The robot is designed and constructed in section 4. Then, section 5 shows the result of the self-balance ability and Lead-through programming. Finally, the conclusion is illustrated in section 6.

2. KINEMATIC MODEL PROBLEM

In previous studies, researchers have taken two simplified 3-DOF robot models into account and proposed two conditions to achieve the balance for serial pitch joints [1].

In general, a gravity torque vector ${}^0\boldsymbol{\tau}$ due to a link mass can be derived from its gravitational force vector ${}^0\boldsymbol{F}$ and its transposed Jacobian matrix ${}^0\boldsymbol{J}$ as in Eq. (1).

$$ {}^0\boldsymbol{\tau} = {}^0\boldsymbol{J}^T \, {}^0\boldsymbol{F} \tag{1}$$

For an ideal anthropomorphic manipulator with parallelogram, the total gravity torque, that each pitch joint has to be affected, was shown separately with respect to the rotation angles θ_2, θ_3, and share a similar equation in Eq. (2).

$$ \tau_i = T_i \cos\theta_i , \; i = 2; 3 \tag{2}$$

Gravity torques are cosine function of rotation angles θ_i and amplitudes of T_i when we have $\theta_i = 0$. To compensate fully gravity torque, original counterbalance mechanisms also have to be capable of producing torques with similar equation. Figure 1 illustrates the original counterbalance mechanism which uses normal spring together with wire, and slider. This mechanism was applied successfully in [4], [5]. The design is as follows.

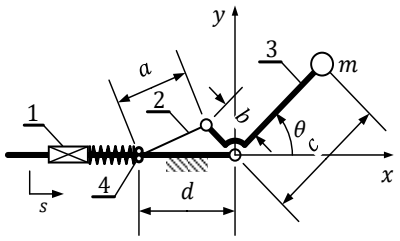

Figure 1. *Original counterbalance mechanism using normal spring, wire and slider*

Given: c, m where $c\ (mm)$ is distance from the mass point to the pivot, $m\ (kg)$ is mass of the link.

Find: b, d, k and s_0 satisfy the relationships in Eqs. (3), (4) and (5).

$$\begin{cases} s_0 = d - b & (3) \\ k = T_m / bd & (4) \\ T_m = mgc & (5) \end{cases}$$

Where: $s_0\ (mm)$ is initial compression length of the spring, $k\ (N/mm)$ is spring stiffness, $b\ (mm)$ and $d\ (mm)$ are design parameters.

However, in the process of designing a robot with the intention of developing further to become a 6-DOF manipulator, a space on link 3 is needed to mount a fourth motor. This leads to an appearance of a distance on the structure of link 3, and can be observed easily in commercial industrial robot arms. The discrepancy in the kinematics model translates into a change of gravity torque equation in term of θ_3, which is expressed as in Eq. (6) in general.

$$\tau_3 = T_3 \cos(\theta_3 + \psi) \tag{6}$$

Where: θ_3 is the rotation angle of link 3, and ψ is phase shift, an abstract value, and can be obtained by simplifying trigonometric expressions.

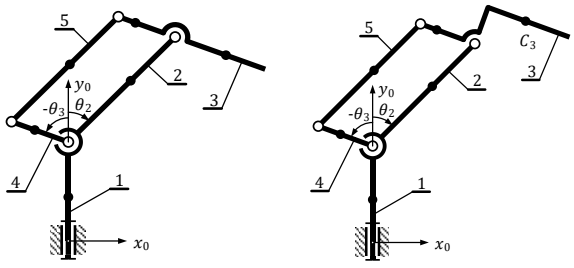

Figure 2. *Kinematic diagram of ideal and real 3-DOF manipulators*

As can be seen from the Eq. (6), a phase shift ψ emerges. We can reduce ψ in order to bring it back to Eq. (2), and combined with the original counterbalance mechanism. However, an equilibrium position always exists that means the robot would return this position after releasing hands. This is because there is always an error in the torque values, which lead to losing the capacity of self-balance.

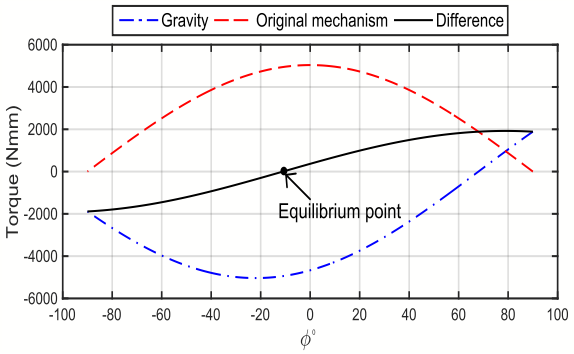

Figure 3. *The torque error due to phase shift*

3. THE PROPOSED IMPROVEMENT FOR A REAL 3-DOF MANIPULATOR

Firstly, we discuss the planar kinematics model of two pitch joints of our robot to obtain gravitational torques equations in detail.

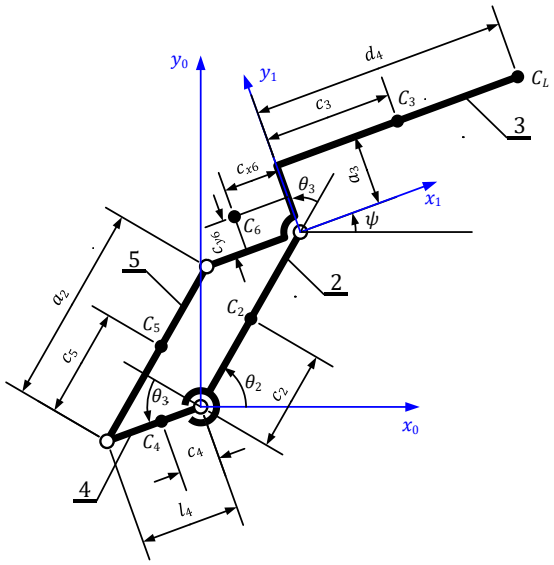

Figure 4. *Kinematic diagram of two pitch joints' robot*

In step 1, we illustrate link 2 and link 3 of the robot by a kinematic diagram, including point masses of these links. In step 2, we determine the coordinates of the point masses in relative to the frame {0}. Note that we create a frame {1} to find the coordinates of C_2, C_6, C_L more easily. In step 3, we look for Jacobian matrix of each coordinate frame and gravitational force vectors. Finally, we apply the Eq. (1) to obtain gravitational torques.

After all the above steps, we have the result as in Eq. (7).

$$\begin{pmatrix}\tau_{G2}\\ \tau_{G3}\end{pmatrix} = \begin{bmatrix} -m_{eq2} g \cos\theta_2 \\ -m_{eq31} g \cos\phi + m_{eq32} g \sin\phi \end{bmatrix} \quad (7)$$

Where:

$$\begin{aligned} \phi &= \theta_2 + \theta_3 - 90^0 \\ m_{eq2} &= m_2 c_2 + (m_3 + m_6 + m_L) a_2 + m_5 c_5 \\ m_{eq31} &= m_3 c_3 - m_4 c_4 - m_5 l_4 + m_6 x_{C6} + m_L d_4 \\ m_{eq32} &= m_3 a_3 + m_6 y_{C6} + m_L a_3 \end{aligned} \quad (8)$$

By applying trigonometric transformation formulas to the second entry, we can achieve the form as Eq. (6).

Let consider a pendulum possessing a similar structure in Figure 5. In the following part, we will look for the proper position for point C on the pendulum so that the error can be canceled. It is clear that $\widehat{LOx} = \theta + \psi$, and gravitational torque

$$\tau_m = T_m \cos(\theta + \psi) \quad (9)$$

Where

$$T_m = mg\sqrt{c^2 + e^2} \quad (10)$$

$$\tan\psi = e/c \quad (11)$$

In comparison with the original mechanism, to produce a sufficient torque, the design also has to satisfy the system equations as shown in section 2 with an additional parameter which is angle ψ. It means that we have to rotate the crank OC an angle of ψ counterclockwise computed from Eq. (11).

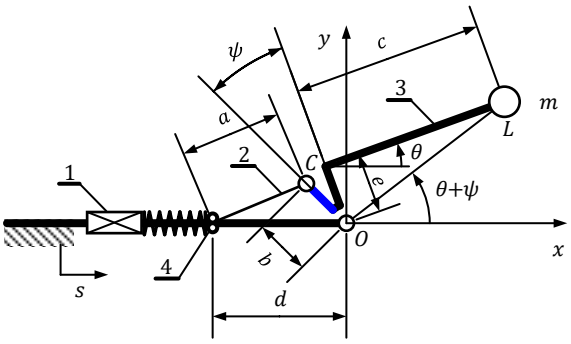

Figure 5. *Diagram of the improved counterbalance mechanism*

4. MODEL DESIGN

4.1 Design of a 3-DOF manipulator

In this section, we show how to construct a three DOF robot arm for pick and place task. The workspace of the robot has to cover a cube of side 200 cm.

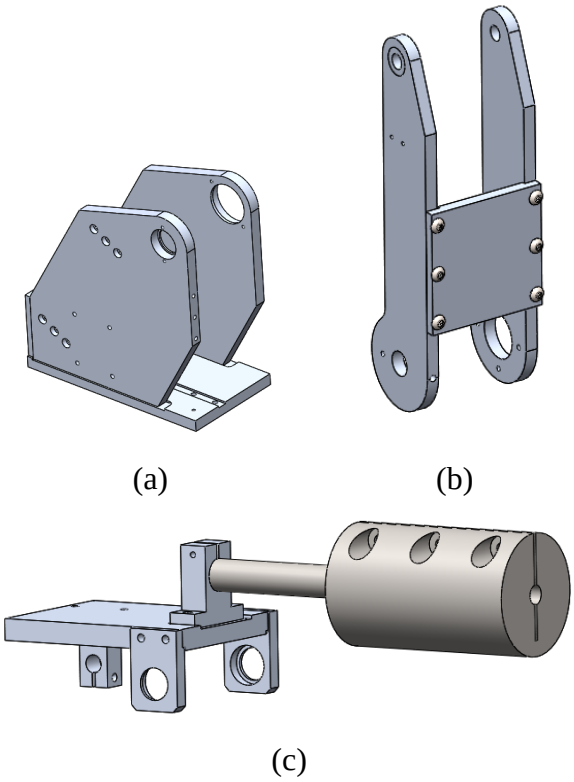

(a) (b)

(c)

Figure 6. *Overall design: (a) link 1, (b) link 2, (c) link 3 and load*

The links lengths are adopted at a particular ratio shown in [6] to optimize the total mass, but still ensure the workability. All links are mainly made of aluminum alloy 6061 plates. The 3 kg-weight fixed load is attached to the end-effector at link 3. Actuators are DC motors, and drive two pitch joints via a pair of 1:1 timing belts. This addition permits the motors to be mounted at lower position in the robot. The motion ranges are $\theta_1 = -170^0 \div 170^0, \theta_2 = 0^0 \div 140^0$, and $\theta_3 = \pm 70^0$, and the workspace is shown in Figure 7.

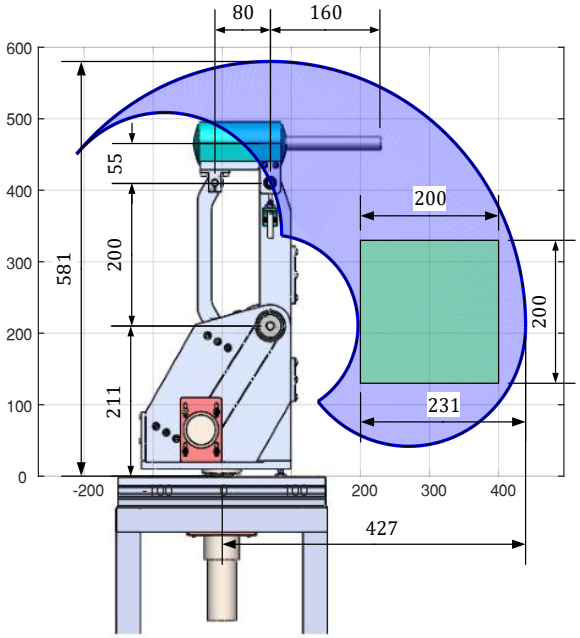

Figure 7. *The workspace of the robot*

4.2 Design of the counterbalance mechanism of the robot

To ensure to achieve the desired workspace, the required springs have to be able to withstand large compression lengths at the maximum rotation angles. The used spring is of MISUMI Corp. with part number SWF26-125, and its specification is shown in Table 1.

Table 1. *Spring Specifications*

Specifications	Values
Spring constant k (N/mm)	5
Free length L (mm)	125
Max deflection (mm)	50

Figure 8 illustrates the elements of the springs' subassembly. The linear shafts are inserted into the springs. To minimize the friction without using bushes, the sliders are

made of bronze while traveling along the linear shafts. Two socket head cap screws are turned to generate the initial deflections. We utilize stainless steel wires. One end is fixed on the slider and the other one will be connected with rotating links.

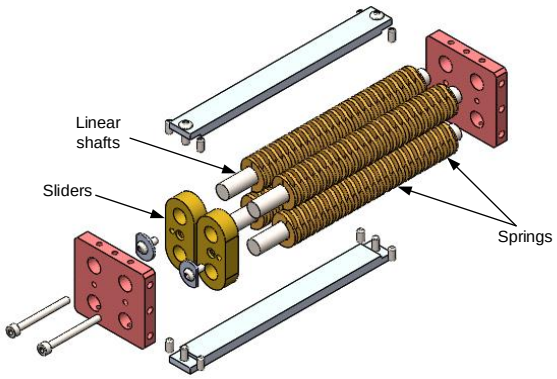

Figure 8. *Springs' subassembly*

Based on the 3D CAD design on SolidWorks, we extract the needed parameters for Eq. (7). They include the links masses and the coordinates of the point masses. By substituting these values into Eq. (7), we obtain

$$\tau_{G2}(\theta_2) = -8260\cos\theta_2 \ \ (Nmm) \tag{12}$$

$$\tau_{G3}(\phi) = -4650\cos\phi + 1936\sin\phi \ \ (Nmm) \tag{13}$$

We can reduce Eq. (13) by employing the trigonometric identity,

$$-a\cos\phi + b\sin\phi = -c\cos(\phi + \psi)$$

Where: $c = \sqrt{a^2 + b^2}, \tan\psi = b/a$

Therefore,

$$\tau_{G3}(\phi) = -5037\cos(\phi + 22) \tag{14}$$

In this case, it is obvious that we cannot cancel the angle of 22^0 to capitalize on the original counterbalance mechanism. The error is considerable, and the robot would return to the equilibrium point shown in Figure 3 instead of maintaining steady at every position as expected, so the improvement is really essential. The parameters of the mechanism are shown in Table 2. While the distances of b are arranged directly on the links, we set d distances on a separate subassembly.

Table 2. *Design parameters of counterbalance mechanism*

	Link 2	Link 3
$u\ (Nmm)$	8260	5037
$d\ (mm)$	46	33
$b\ (mm)$	18	15
$s_0\ (mm)$	28	18

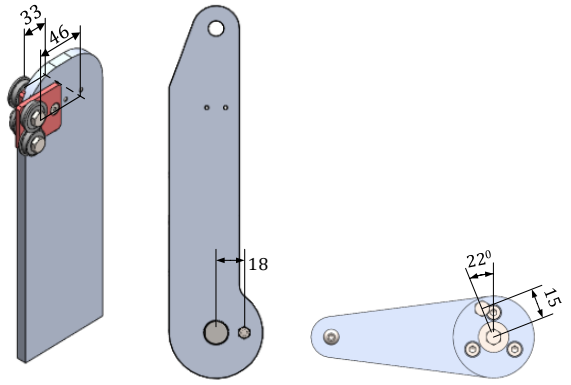

(a) (b) (c)

Figure 9. *(a) d distances, (b), (c) b distances*

5. EXPERIMENT

5.1 Self-balance verification

The prototype has been constructed, and the counterbalance mechanism is attached. As a result, the mechanism has worked efficiently. We can move manually the end-effector with ease. Despite of the heavy load, the robot is able to stand still at any postures in its workspace without auxiliary actuators or brakes, even at the maximum horizontal reach.

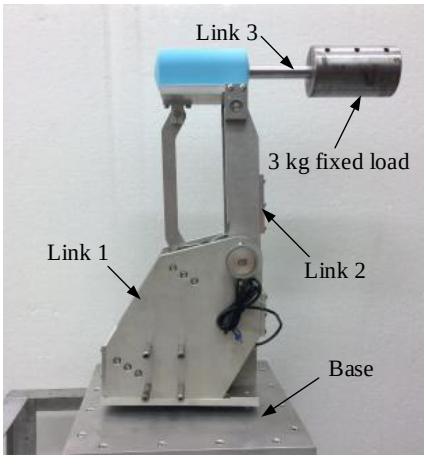

Figure 10. *The prototype of the manipulator*

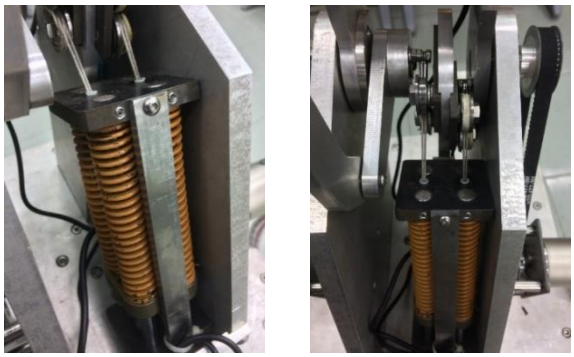

Figure 11. *The counterbalance mechanism*

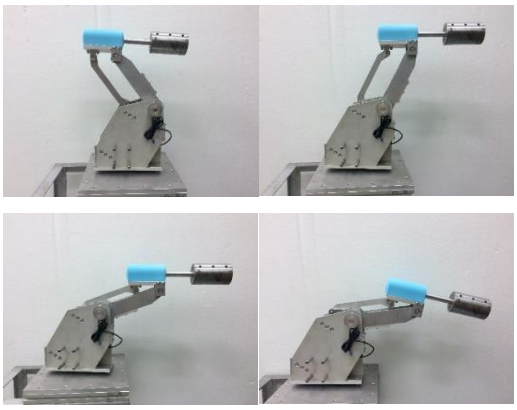

Figure 12. *The ability of self-balance*

Figure 10 shows the prototype of the designed robot. Figure 11 shows a real counterbalance mechanism. Figure 12 shows a few positions of the robot that can do self-balance.

5.2 Lead-through programming

Figure 13 shows the electrical system. The central microcontroller is dsPIC30F4011. "Home" position is set by proximity sensors.

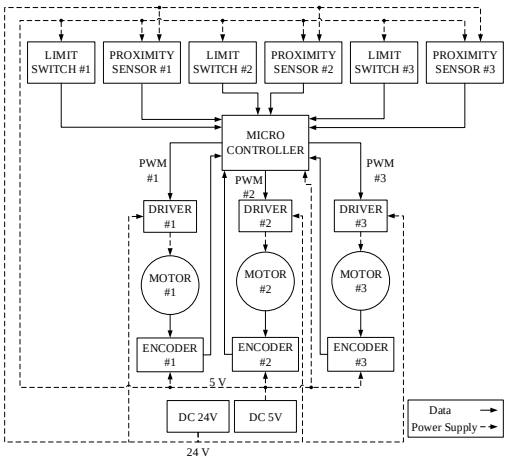

Figure 13. *Electrical system diagram*

There are five main operating stages, being illustrated in Figure 14. Control signals of the modes are sent to the microcontroller via RS-232 communication with a computer. Due to optical encoders attached to the motors, the "STARTING_HOME" stage runs an algorithm to find a defined home position before being ready to work. In the "LEAD-THROUGH" stage, the robot is available to record desired points by pressing a button on a computer interface. The robot moves automatically all recorded points respectively in "PLAY_BACK" stage.

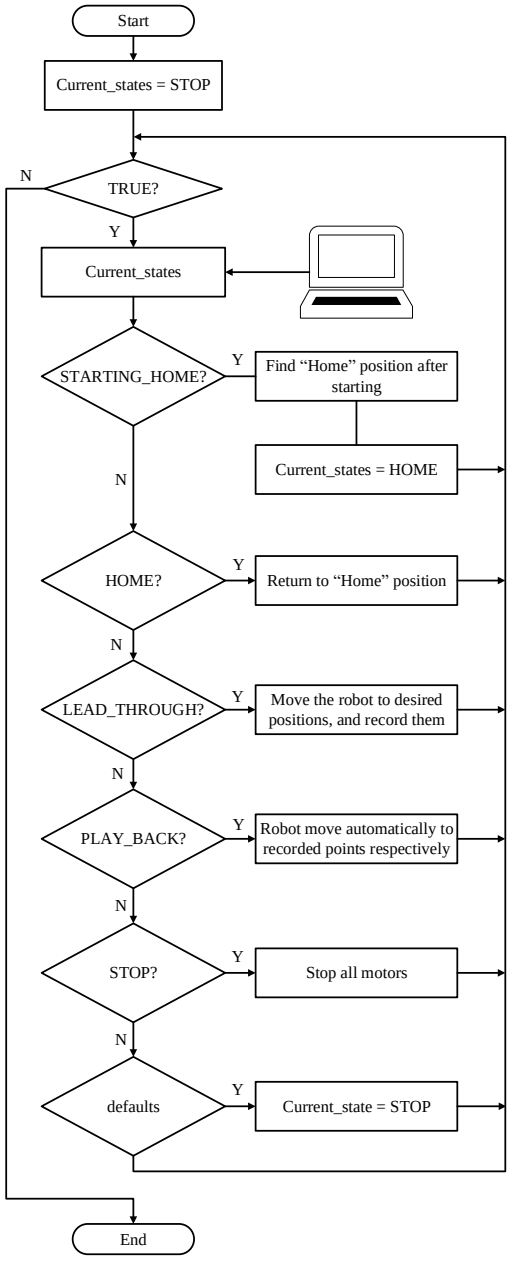

Figure 14. *The control algorithm for Lead-through programming*

To verify the Lead-through programming, a pen is attached to the end-effector. There are two pre-defined points on a table. The robot is moved manually from the first defined point to the second one. In the process of moving the robot, some intermediate points are chosen randomly between the initial and final points and shown in Figure 15.

In the experiment, we can move the robot easily by pulling the end-effector of the robot. This shows the advantage of our design compared with several complex robot structures. Users can teach the robot efficiently just by simple motions.

Figure 15. *The robot is moved manually to separate points, and record them.*

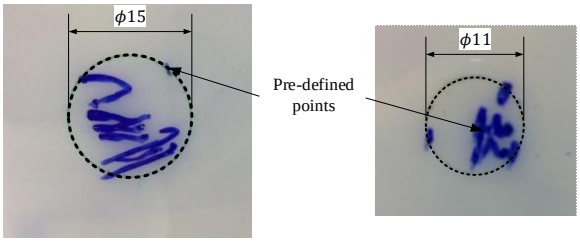

Figure 16. *Repeatability of the robot*

The repeatability of the robot is shown in Figure 16. We get these results by controlling the robot to move between two pre-defined points. These values are respectively 15mm and 11mm. The repeatability is quite considerable. The reason is that there is a backlash in gearboxes, resulting to free movements which are out of control after the motors complete controlled angles. Besides, the controller is not good enough to remain the same values of rotating angles through the encoders after every repeat. The errors are cumulative and create significant repeatability.

6. CONCLUSION

In this paper, based on a practical problem in designing a robot applied Lead-through programming, we have improved the original counterbalance mechanism to cancel completely the gravitational torque errors while carrying a 3kg concentrated weigh representing for last three joints. The influence of the improved counterbalance mechanism was verified directly with the constructed robot. The improvement is useful to other counterbalance mechanisms. In the future, we will develop a reliable controller for the robot to improve their performance, and then replace the fixed load with three last joints to become a full 6 DOF robot.

ACKNOWLEDGEMENT

This research is funded by Vietnam National University Ho Chi Minh City (VNU-HCM) under grant number C2017-20-04.

REFERENCES

[1] Kuk-Hyun Ahn, Won-Bum Lee, and Jae-Bok Song, *Reduction in Gravitational Torques of an Industrial Robot Equipped with 2 DOF Passive Counterbalance Mechanisms*, IEEE/RSJ International Conference on Intelligent Robots and Systems (IROS 2016), pp. 4344 – 4349, Daejeon, Korea, 2016.

[2] Gen Endo, Hiroya Yamada, Akira Yajima, Masaru Ogata, and Shigeo Hirose, *A Passive Weight Compensation Mechanism with a Non-Circular Pulley and a Spring*, IEEE International Conference on Robotics and Automation 9ICRA 2010), pp.3843 – 3848, Alaska, USA, 2010.

[3] Nathan Ulrich, and Vijay Kumar, *Passive Mechanical Gravity Compensation for Robot Manipulators*, Proceedings of the 1991 IEEE International Conference on Robotics and Automation, pp. 1536 – 1541, California, USA, 1991.

[4] Hwi-Su Kim, and Jae-Bok Song, *Multi-DOF Counterbalance Mechanism for a Service Robot Arm*, IEEE/ASME Transactions on Mechatronics, Vol. 19, No. 6, pp. 1756-1763, 2014.
[5] Vigen H. Arakelian, and Sébastien Briot, *Balancing of Linkages and Robot Manipulators*, Springer, 2015.
[6] Lelai Zhou, Shaoping Bai, and Michael Rygaard Hansen, *Integrated dimensional and drive-train design optimization of a light-weight anthropomorphic arm*, Robotics and Autonomous Systems, Vol. 60, pp. 113-122, 2012.

***Corresponding author*:**
Phung Tri Cong
Ho Chi Minh City University of Technology, VNU-HCM
Email: ptcong@hcmut.edu.vn